Supporting Information

Pt_{17} Nanocluster Electrocatalysts: Preparation and Origin of High Oxygen Reduction Reaction Activity

Tokuhisa Kawawaki,[‡,a,b,c] Yusuke Mitomi,[‡,a] Naoki Nishi,[a] Ryuki Kurosaki,[a] Kazutaka Oiwa,[a] Tomoya Tanaka,[a] Hinoki Hirase,[d] Sayuri Miyajima,[a] Yoshiki Niihori,[b] D. J. Osborn,[f] Takanori Koitaya,[c,e] Gregory F. Metha,[f] Toshihiko Yokoyama,[c,e] Kenji Iida,[*,d] and Yuichi Negishi[*,a,b]

[a] Department of Applied Chemistry, Faculty of Science, Tokyo University of Science, Kagurazaka, Shinjuku-ku, Tokyo 162−8601, Japan.
[b] Research Institute for Science & Technology, Tokyo University of Science, Kagurazaka, Shinjuku-ku, Tokyo 162−8601, Japan.
[c] Physical and Chemical Research Infrastructure Group, RIKEN SPring-8 Center, RIKEN, Sayo, Hyogo 679−5198, Japan.
[d] Institute for Catalysis, Hokkaido University, Sapporo, Hokkaido 001−0021, Japan.
[e] Institute for Molecular Science, Okazaki, Aichi 444−8585, Japan.
[f] Department of Chemistry, University of Adelaide, Adelaide, South Australia, 5005, Australia
[‡] These authors contributed equally to this work.
*E-mail: k-iida@cat.hokudai.ac.jp (K. Iida); negishi@rs.tus.ac.jp (Y. Negishi)

S1. Experimental Section

S1.1. Chemicals

All chemicals were commercially obtained and used without further purification. $H_2PtCl_6 \cdot 6H_2O$ was purchased from Tanaka Kikinzoku (TKK, Tokyo, Japan). Sodium hydroxide (NaOH), PPh_3, Pt standard solution (1000 mg/L), bismuth (Bi) standard solution (1000 mg/L), ultrapure water (18.2 MΩ cm), 2-propanol, and Nafion^{TM} were obtained from FUJIFILM Wako Pure Chemical Corporation (Osaka, Japan). Acetone, acetonitrile, dichloromethane, ethylene glycol, perchloric acid, methanol, nitric acid, and toluene were sourced from Kanto Chemical Co., Inc. (Tokyo, Japan). Ketjen black (EC300J) was from Lion Specialty Chemicals Co., Ltd. (Tokyo, Japan). Commercial Pt NPs/carbon black (CB; TEC10E50E) was from Tanaka Kikinzoku. *Trans*-2-[3-(4-*tert*-butylphenyl)-2-methyl-2-propenylidene]malononitrile (DCTB) was from Tokyo Chemical Industry Co. Ltd. (TCI, Tokyo, Japan). Alumina paste (ALUMINA POLISHINNG SUSPENSION) was from Maruto Instrument Co., Ltd. (Tokyo, Japan).

S1.2. Synthesis of $[Pt_{17}(CO)_{12}(PPh_3)_8]Cl_n$ (n = 1,2)

$[Pt_{17}(CO)_{12}(PPh_3)_8]Cl_n$ was synthesized using the method reported in our previous study[1] with slight modifications (Figs. S4 and S36). First, $H_2PtCl_6 \cdot 6H_2O$ (156 mg) and NaOH (90 mg, 2.2 mmol) were dissolved in ethylene glycol (25 mL). NaOH was used to control the pH of the solution and thereby suppress the particle size obtained by polyol reduction. Then, the mixture was heated and stirred at 120 °C for 8 min and 45 s to reduce Pt ions and produce CO catalyzed by Pt ions. The solution changed from yellow to dark brown. After cooling to room temperature (25 °C), using an ice bath, acetone (10 mL) containing PPh_3 (1.26 g, 2.0 mmol) was promptly added. After 5 min, a mixture of water (~10 mL) and toluene (~7 mL) was added to the reaction solution. The resulting Pt NCs including $[Pt_{17}(CO)_{12}(PPh_3)_8]Cl_n$ were transferred to the organic phase. Then, the organic phase was separated from the water phase and dried with a rotary evaporator. The dried product was washed with water and then methanol to eliminate ethylene glycol and excess PPh_3. At this stage, the product was a mixture of clusters of several sizes and was thus washed with acetonitrile and toluene. The product was dried and the target $[Pt_{17}(CO)_{12}(PPh_3)_8]Cl_n$ was extracted from the dried mixture with dichloromethane.

S1.3. Preparation of Pt_{17}/CB(1.0 wt% Pt) and Pt NPs/CB(1.0 wt% Pt)

For these syntheses, Ketjen black, a highly conductive CB, was used as CB because it is also used in commercial Pt NPs/CB (TEC10E50E). To prepare Pt_{17}/CB(1.0 wt% Pt), $[Pt_{17}(CO)_{12}(PPh_3)_8]Cl_n$ was first adsorbed on CB by mixing a dichloromethane solution containing $[Pt_{17}(CO)_{12}(PPh_3)_8]Cl_n$ (1.2 mg) with a dichloromethane solution containing CB (EC300J) (60 mg) for 2 h at room temperature. The total volume of the solution was fixed at 30 mL, and the mixing ratio of $[Pt_{17}(CO)_{12}(PPh_3)_8]Cl_n$ to CB was fixed at 1.0 wt% Pt. The amount of Pt in the solution was confirmed by ICP-MS. After mixing for 24 h, the solution became colorless, which indicated that almost all the $[Pt_{17}(CO)_{12}(PPh_3)_8]Cl_n$ were adsorbed on CB ($Pt_{17}(CO)_{12}(PPh_3)_8$/CB(1.0 wt% Pt)). After adsorption, the obtained $Pt_{17}(CO)_{12}(PPh_3)_8$/CB was calcined under reduced pressure ($<1.0 \times 10^{-1}$ Pa) to remove PPh_3 ligands. The furnace temperature was increased at a rate of 7 °C/min and then maintained at 200 °C for 80 min (Fig. S13). To prepare Pt NPs/CB(1.0 wt% Pt), commercial Pt NPs/CB(46.9 wt% Pt) was mixed with CB to reduce the weight percentage of Pt from 46.9 to

1.0 wt%.

S1.4. Preparation of Pt_{17}/CB(20.0 wt% Pt)

Pt_{17}/CB(20.0 wt% Pt) was prepared by the impregnation method. The Pt_{17} cluster dichloromethane solution was dropped on the Ketjen black and then the catalysts was dried. The ligands were then removed by calcination at 250 °C for 120 min to obtain Pt_{17}/CB(20.0 wt% Pt)-EC.

S1.5. Preparation of catalyst slurry

To conduct the electrochemical measurements on Pt_{17}/CB(1.0 wt% Pt), Pt_{17}/CB(20.0 wt% Pt), Pt NPs/CB(1.0 wt% Pt), and Pt NPs/CB(46.9 wt% Pt), a catalyst slurry was prepared as follows (Fig. S37)[2]. First, the catalyst powder (10.1 mg; Pt_{17}/CB(1.0 wt% Pt), 12.5 mg; Pt_{17}/CB(20.0 wt% Pt), 10.1 mg; Pt NPs/CB(1.0 wt% Pt), or 18.8 mg; Pt NPs/CB(46.9 wt% Pt)) was dispersed in a solution containing H_2O (19.1 mL) and 2-propanol (6.0 mL). Then, Nafion^{TM} solution (100 µL) was added to this solution. The vial containing this mixture was sealed and ultrasonicated for 60 min in an ice bath.

S1.6. Electrochemical measurements

All electrochemical measurements were performed using a CHI710D electrochemical workstation (ALS, Osaka, Japan) with a RRDE-3A rotating ring disk electrode apparatus (BAS, Tokyo, Japan). A rotating disk electrode (RDE, diameter = 5 mm) was polished with an alumina paste and then sonicated in water before usage. A Pt coil electrode was used as the counter electrode. A reversible hydrogen electrode (RHE) was used as the reference electrode.

In the experiment, first, the catalyst slurry was sonicated in an ice bath for 60 min. Then, the catalyst slurry (10 µL) was carefully dropped onto the RDE by the drop-cast method. The electrode was then dried by rotating it at 700 rpm. After the catalyst slurry was sufficiently dried, each electrode was set in an electrochemical measurement system containing $HClO_4$ solution (0.10 mol/L, pH = 1.0) as electrolyte (Fig. S38). The electrodes were then cleaned by bubbling N_2 gas for 30 min, followed by cyclic voltammetry (CV) 50 times in the region of 0.00–1.20 V (vs. RHE) at a scanning rate of 500 mV/s. Subsequently, CV was performed 3 cycles at a rate of 50 mV/s in the region of 0.00–1.20 V (vs. RHE) to evaluate ECSA. After CV, LSV was performed at a rate of 10 mV/s in the region of 0.10–1.10 V (vs. RHE) under N_2 atmosphere. Then, the LSV measurements were also performed at a rate of 10 mV/s in the range of 0.10–1.10 V (vs. RHE) under an O_2 atmosphere while the RDE was rotated at 400, 900, 1600, and 2500 rpm. Finally, the background measured in N_2-saturated solution is subtracted from the LSV measured in O_2-saturated solution.

Durability was measured by degrading the catalyst through continuous cycles of load-response simulated potential cycles (Fig. S39). Cyclic voltammetry was measured at the end of 10,500 cycles, and the rate of decrease in ECSA was calculated to compare durability.

S1.7. Characterization

Matrix-assisted laser desorption/ionization (MALDI)-MS spectra were recorded on a JMS-S3000 spiral time-of-flight mass spectrometer (JEOL, Tokyo, Japan) equipped with a semiconductor laser (λ = 349 nm). DCTB was used as the MALDI matrix. To minimize NC dissociation induced by laser irradiation, the NC-to-matrix ratio was fixed at 1:1000.

ESI-MS was performed on a micrOTOF II reflectron time-of-flight mass spectrometer (Bruker, Boston, MA, USA). For the measurements, a NC solution with a concentration of ~10 µg/mL in dichloromethane was electrosprayed at a flow rate of 180 µL/h.

ICP-MS was performed on an Agilent 7850c spectrometer (Agilent Technologies, Tokyo, Japan). Bi was used as the internal standard. Pt standard solution was used to obtain the calibration line. The ICP-MS measurements were performed on the solution before and after mixing $[Pt_{17}(CO)_{12}(PPh_3)_8]Cl_n$ with CB to estimate the adsorbed or loaded Pt content.

TEM images were recorded on a H-9500 electron microscope (HITACHI, Tokyo, Japan) or JEM-2100 electron microscope (JEOL, Tokyo, Japan) operating at 200 kV, and typically using a magnification of 600,000. A NP-C15 (Okenshoji, Tokyo, Japan) was used as a copper microgrid.

The high-angle annular dark field scanning TEM (HAADF-STEM) images were obtained by ultra-high-resolution transmission electron microscope (The FEI Titan Themis 80–200) operating at 200 kV, with a beam convergence semi angle of 25 mrad and HAADF collection angle from 56–200 mrad.

FT-IR spectra of the product were obtained using the attenuated total reflectance (ATR) method in the region between 400 and 4000 cm^{-1} on an FT/IR-4600-ATR-PRO ONE spectrometer (JASCO, Tokyo, Japan) equipped with a DLATGS detector. The average number of scans and resolution used for the measurements were 50 and 4 cm^{-1}, respectively.

Pt L_3-edge XAFS measurements were performed at the beamline BL01B1 of the SPring-8 facility of the Japan Synchrotron Radiation Research Institute (proposal numbers 2020A0695, 2021A1102, 2021B1163, and 2022A1075). The incident X-ray beam was monochromatized by a Si(111) double-crystal monochromator. As references, XAFS spectra of all samples were recorded in transmission mode using ionization chambers. The X-ray energies for the Pt L_3-edges were calibrated using Pt foil. The XANES and EXAFS spectra were analyzed using xTunes as follows. The χ spectra were extracted by subtracting the atomic absorption background using cubic spline interpolation and normalized to the edge height. The normalized data were used as the XANES spectra. The k^3-weighted χ spectra in the k range of 3.0–14.0 Å^{-1} for the Pt L_3-edge were Fourier-transformed into r space for structural analysis.

HAX-PES measurements were performed on a Scienta-Omicron R4000 HiPP-2[3] equipped with a differential pumping system installed at the undulator beamline BL36XU[4] in SPring-8 that provides intense hard X-ray microbeam[5]. The X-rays were monochromatized by two sets of Si(111) channel-cut monochromator crystals and the photon energy employed the HAX-PES measurements was 7.94 keV using 444 reflections. The X-ray spot size at the measurement position was reduced to 70 µm (vertical) × 28 µm (horizontal) by the focusing mirrors using a front cone with an aperture diameter of 50 µm.

Thermogravimetric analysis (TGA) was conducted on a TGA2000SA (Bruker, Boston, MA, USA) and at a heating rate of 5 °C/min (from room temperature to 900 °C) under N_2 atmosphere.

S2. Calculation

Spin-polarized DFT calculations were performed using the Quantum Espresso program package with the Perdew–Burke–Ernzerhof functional and the empirical dispersion correction (PBE-D3)[6–9]. In the calculations, the cutoff energy for the plane-wave basis was 50 Ry and a 2 × 2 × 1 k-point mesh was used. The free energy change (ΔG) was given by $\Delta G = \Delta E + \Delta E_{\mathrm{ZPE}} - T\Delta S$ based on the theoretical model proposed by Nørskov et al.[10] Here, ΔE is the total energy change obtained from the DFT calculation, ΔE_{ZPE} is the change in zero-point energy, T is temperature (298.15 K), and ΔS is the change in entropy. The effect of a bias was added by shifting the free energy by $-eU$, where e is the elementary charge and U is the electrode potential. For OOH* and O_2* species, we utilized the sum of O* + OH*[11] and O* + O* for $\Delta E_{\mathrm{ZPE}} - T\Delta S$, respectively. The energy of the free O_2 molecule was estimated from the experimental value of the reaction energy of $1/2O_2 + 2H^+ + 2e^- \rightarrow H_2O$ because the high-spin ground state of O_2 cannot be well reproduced using the conventional DFT method.[10] We consider that the present correction is enough to describe the free energy diagram because the amount of the correction for $\Delta E_{\mathrm{ZPE}} - T\Delta S$ is different by only less than 0.15 eV compared to that for the O_2 reduction on the Pt_{13}/graphene system.[12]

S3. Additional Tables

Table S1. Potential Assignment of the Peaks in Fourier Transform Infrared Spectroscopy (FT-IR) Spectra for the $[Pt_{17}(CO)_{12}(PPh)_8]^z$, $Pt_{17}(CO)_{12}(PPh)_8$/CB, and Pt_{17}/CB

Wavenumber (cm^{-1})	Assignment [a]	Spectrum [a]
3054.7	ν(C—H) aromatic [b]	$[Pt_{17}(CO)_{12}(PPh)_8]^z$
2158.0	C=C=O	$Pt_{17}(CO)_{12}(PPh)_8$/CB Pt_{17}/CB
2028.7	terminal CO	$Pt_{17}(CO)_{12}(PPh)_8$/CB Pt_{17}/CB
1974.8	terminal CO	$Pt_{17}(CO)_{12}(PPh)_8$/CB Pt_{17}/CB
1973.8	terminal CO	$[Pt_{17}(CO)_{12}(PPh)_8]^z$
1941.9	terminal CO	$[Pt_{17}(CO)_{12}(PPh)_8]^z$
1742.4	bridge CO	$[Pt_{17}(CO)_{12}(PPh)_8]^z$
1572.7	ν(C—H) aromatic [b]	$[Pt_{17}(CO)_{12}(PPh)_8]^z$ $Pt_{17}(CO)_{12}(PPh)_8$/CB Pt_{17}/CB
1478.2	ν(C—H) aromatic [b]	$[Pt_{17}(CO)_{12}(PPh)_8]^z$
1435.7	ν(C—H) aromatic [b]	$[Pt_{17}(CO)_{12}(PPh)_8]^z$
1303.5	ν(P=O)	$Pt_{17}(CO)_{12}(PPh)_8$/CB Pt_{17}/CB
1095.3	$\delta(C—H)_{ip}$ [b]	$[Pt_{17}(CO)_{12}(PPh)_8]^z$ $Pt_{17}(CO)_{12}(PPh)_8$/CB
740.5	δ(C—H) [b]	$[Pt_{17}(CO)_{12}(PPh)_8]^z$ $Pt_{17}(CO)_{12}(PPh)_8$/CB Pt_{17}/CB
691.4	$\delta(C—H)_{oop}$ ring [b]	$[Pt_{17}(CO)_{12}(PPh)_8]^z$ $Pt_{17}(CO)_{12}(PPh)_8$/CB Pt_{17}/CB

[a] See ref. 13. [b] see Fig. 3 and S10. [c] ν: stretching, δ: deformation, ip: in-plane, oop: out-of-plane.

Table S2. Curve Fitting Analysis of Pt L_3-edge EXAFS Data for Pt_{17}/CB(1.0 wt% Pt)

Bond	C. N. [a,b]	R(Å) [a]	D. W. [a,c]	R factor (%) [a]
Pt−Pt	3.4(4)	2.64(8)	0.10(4)	4.5
Pt−C	2.0(3)	2.03(6)	0.07(6)	

The numbers in parentheses are uncertainties; 3.4(4) and 2.64(8) represent 3.4 ± 0.4 and 2.64 ± 0.08, respectively. [a] These values were obtained by fitting with Pt−Pt and Pt−C bonds. [b] Coordination number. [c] Debye−Waller factor.

Table S3. Half-Wave Potential for Pt_{17}/CB(1.0 wt% Pt)-EC

Revolution per minute	Half-wave potential (V) [a]
2500	0.628
1600	0.670
900	0.706
400	0.741

[a] See Fig. 5(a).

Table S4. Half-Wave Potential for Pt_{17}/CB(1.0 wt% Pt)-EC

Revolution per minute	Half-wave potential (V) [a]
2500	0.523
1600	0.589
900	0.635
400	0.686

[a] See Fig. 5(b).

Table S5. Results of Density Functional Theory (DFT) Calculations for O_2/Pt_{17}/graphite(*X*)

X site [a]	E_{O2ads} (eV) [b]	Pt—Pt length (Å)	Pt—O length (Å)	O—O length (Å) [c]
A	−1.65	2.60	1.97	1.39
B	−2.01	2.62	1.96	1.43
C	−1.63	2.53	1.93	1.43
D	−2.21	3.47	1.95	1.40

[a] See Fig. 6(a). [b] $E_{\mathrm{O2ads}} = O_2/Pt_{17}/\mathrm{graphite} - (Pt_{17}/\mathrm{graphite} + O_2)$. [c] 1.23 Å before the adsorption.

Table S6. Results of DFT Calculations for (O + OH)/Pt_{17}/graphite(*X*)

X site [a]	E_{HO2ads} (eV)	Pt—Pt length (Å)	Pt—OH length (Å)	Pt—O length (Å)	O—O length (Å)	O—H (Å)
A	−2.76	2.62	1.98	1.83	1.39	0.992 1.88
B	−4.12	2.70	1.92	1.80	1.43	0.992 1.99
C	−3.54	2.55	1.94	1.77	1.42	0.977 −
D	−3.85	3.83	1.93	1.77	1.40	0.979 −

[a] See Fig. 6(a). [b] $E_{\mathrm{HO2ads}} = (O + OH)/Pt_{17}/\mathrm{graphite} - (Pt_{17}/\mathrm{graphite} + O_2 + \frac{1}{2} H_2)$.

S4. Additional Figures

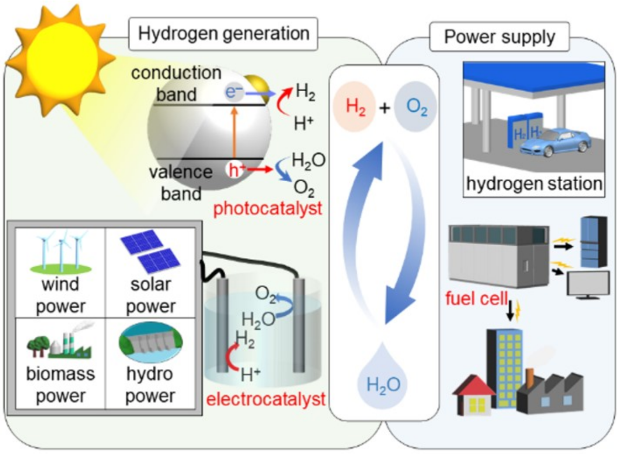

Fig. S1 Schematic of the energy conversion system expected for constructing a sustainable society. Note that sunlight also produces wind, biomass, and hydro power in addition to solar power. Reproduced with permission from ref. 14. Copyright 2021 The Royal Society of Chemistry.

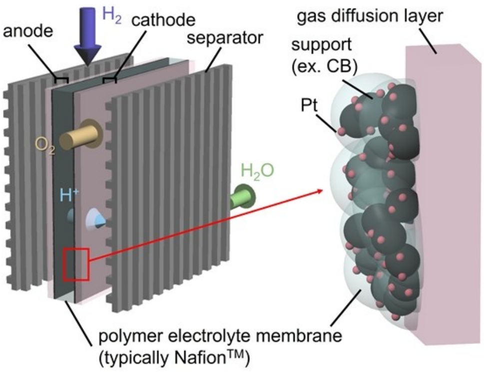

reaction on the electrode

cathode : $O_2 + 4H^+ + 4e^- \rightarrow 2H_2O$

anode : $2H_2 \rightarrow 4H^+ + 4e^-$

total reaction : $2H_2 + O_2 \rightarrow 2H_2O$

Fig. S2 Schematic of a polymer electrolyte fuel cell (PEFC) and the reaction at the electrode: Reproduced with permission from ref. 2. Copyright 2021 The Royal Society of Chemistry.

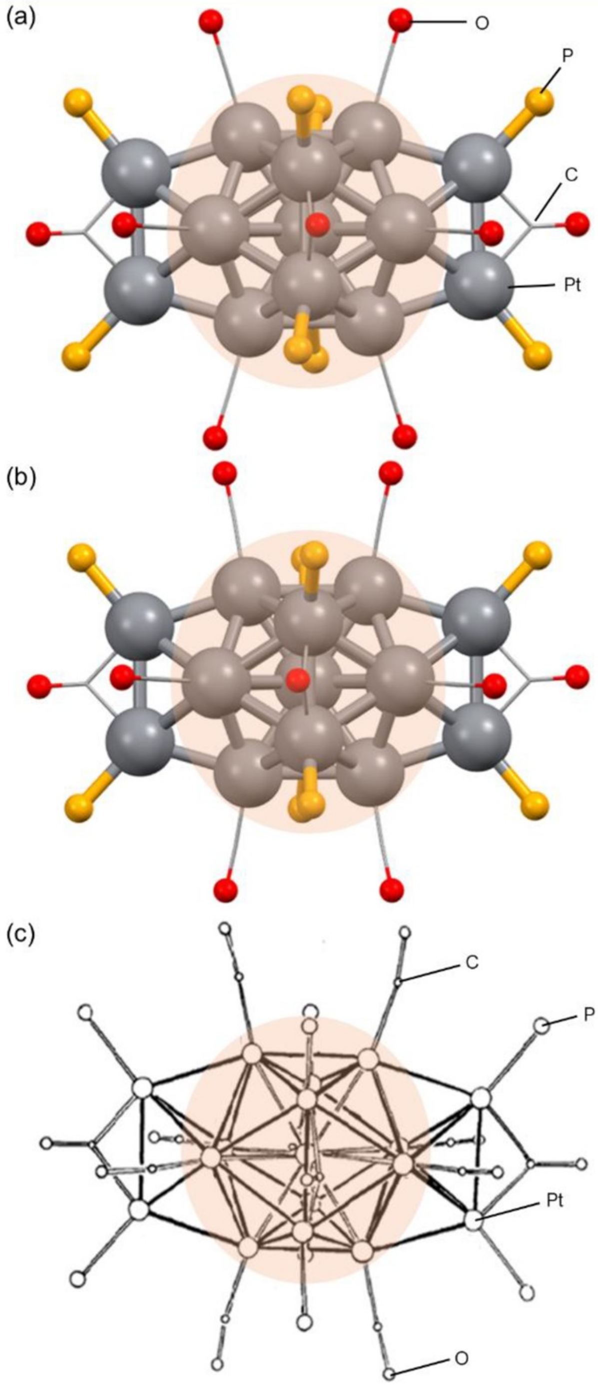

Fig. S3 Geometry of Pt_{17} NCs: (a) $[Pt_{17}(CO)_{12}(PPh_3)_8][SbF_6]$.[1] (b) $[Pt_{17}(CO)_{12}(PPh_3)_8][(SbF_6)_2]$.[1] (c) $[Pt_{17}(CO)_{12}(PEt_3)_8]^0$ (PEt_3 = triethylphosphine)[15]. A red circle highlights an icosahedral Pt_{13} core in Pt_{17} NCs. Reproduced with permission from ref. 1 and 15. Copyright 1989 Elsevier.

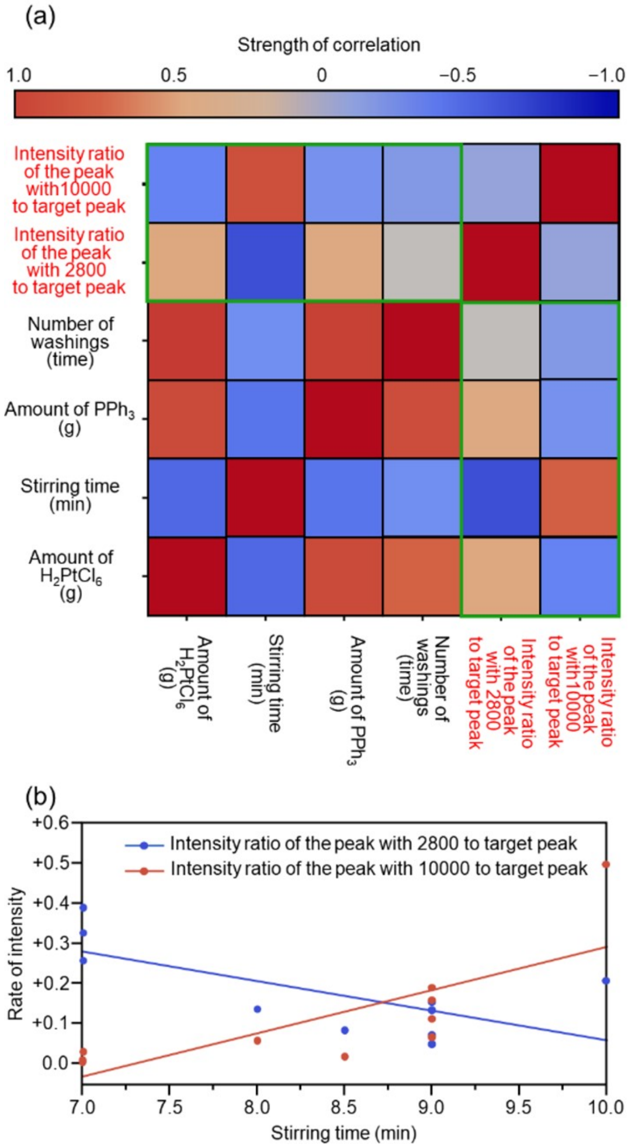

Fig. S4 Exploration of the best condition for the selective synthesis of Pt_{17} NCs: (a) Heat map analysis for understanding of the effect of each experimental condition (amounts of H_2PtCl_6, stirring time, amounts of PPh_3 and the number of the washings) on the relative intensity of the byproduct with m/z = ~2800 or 10000 to the target products with m/z = ~4200 (Pt_{17} NCs) in the matrix-assisted laser desorption/ionization (MALDI) mass spectrum. In this heat map, the color of the panel in the green square is important. The result indicates that 1) the stirring time is most strongly correlate with the relative intensity of the Pt_{17} NCs in the MALDI, namely, delicate parameter, and 2) the longer the stirring time, the weaker the intensity of the byproduct peaks around m/z = ~2800 and the stronger the intensity of the byproduct peaks around m/z = ~10000. (b) Relation between the stirring time and the relative intensity of the byproducts (m/z = ~2800 or 10000) to the Pt_{17} NCs (m/z = ~4200). These results guided us to select the stirring time of 8 minutes and 45 seconds for the selective synthesis of the objective Pt_{17} NCs. The other parameters (amounts of H_2PtCl_6, amounts of PPh_3 and the number of the washings) are also optimized, similarly to the stirring time.

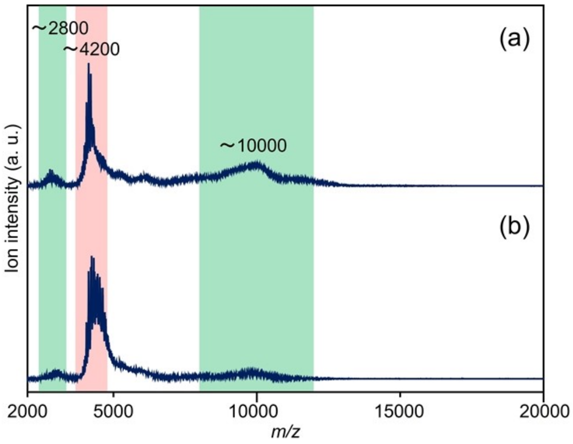

Fig. S5 Comparison of MALDI mass spectra between our previous and present studies: (a) MALDI mass spectrum obtained in our previous study (0.10 mmol for the amounts of H_2PtCl_6, 9 minutes for stirring time and 2.0 mmol for amounts of PPh_3). (b) MALDI mass spectrum obtained in our present study (0.30 mmol for the amounts of H_2PtCl_6, 8.75 minutes (8 minutes and 45 seconds) for stirring time and 4.8 mmol for amounts of PPh_3). The present study increased 3.8 folds the yield of the objective Pt_{17} NCs.

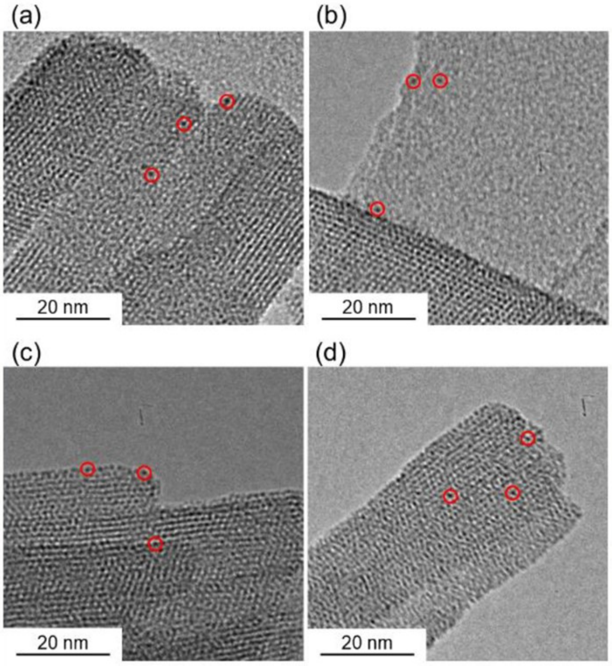

Fig. S6 Transmission electron microscope (TEM) images of $[Pt_{17}(CO)_{12}(PPh_3)_8]^z$ (z = 1+ or 2+): (a–d) Different views from Fig. 2(a). In this TEM images, the parallel line is not due to the lattice fringes of Pt_{17} cluster but due to the collodion membrane on the TEM grid.

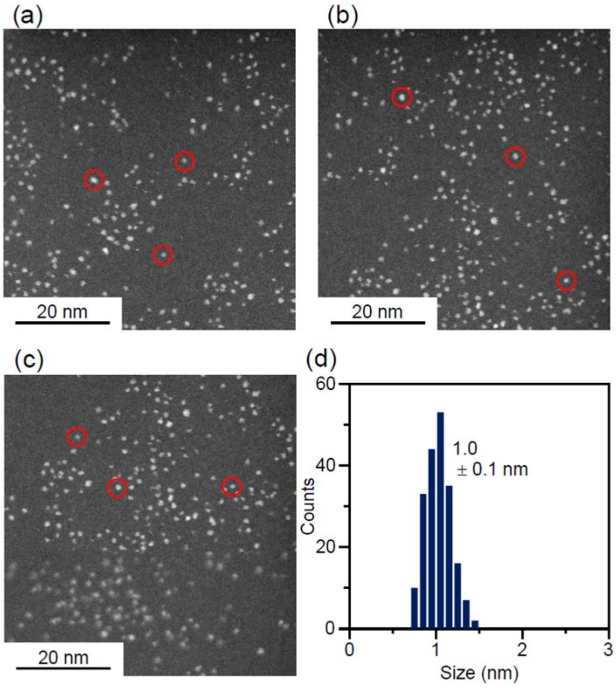

Fig. S7 High-angle annular dark field scanning TEM (HAADF-STEM) images and the histogram of $[Pt_{17}(CO)_{12}(PPh_3)_8]^z$ (*z* = 1+ or 2+). Overall, the particle sizes are similar to those in Figure S6.

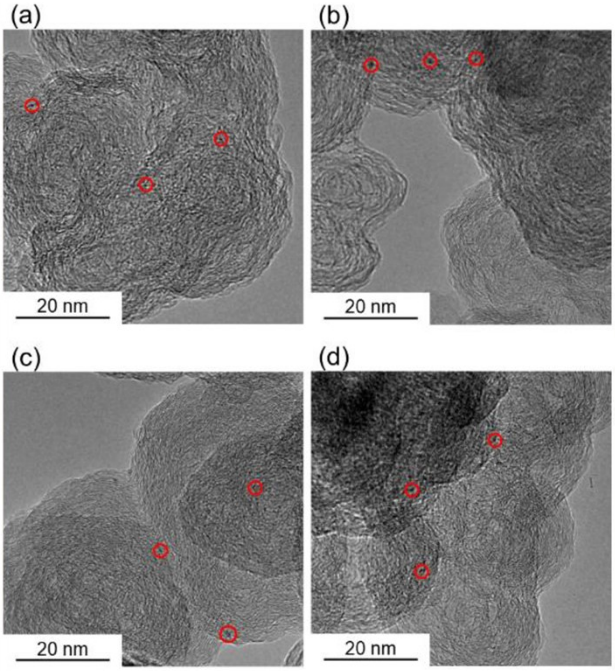

Fig. S8 TEM images of $Pt_{17}(CO)_{12}(PPh_3)_8$/CB. (a−d) Different views from Fig. 2(b).

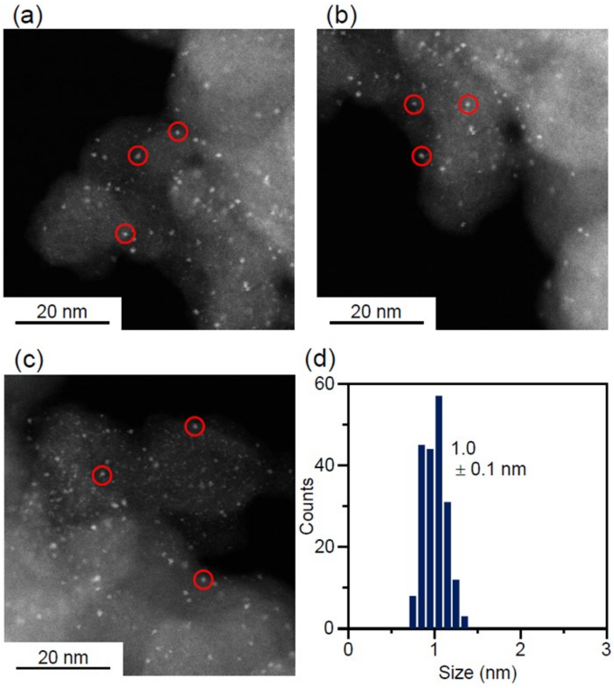

Fig. S9 HAADF-STEM images and the histogram of $Pt_{17}(CO)_{12}(PPh_3)_8$/CB. Overall, the particle sizes are similar to those in Figure S8.

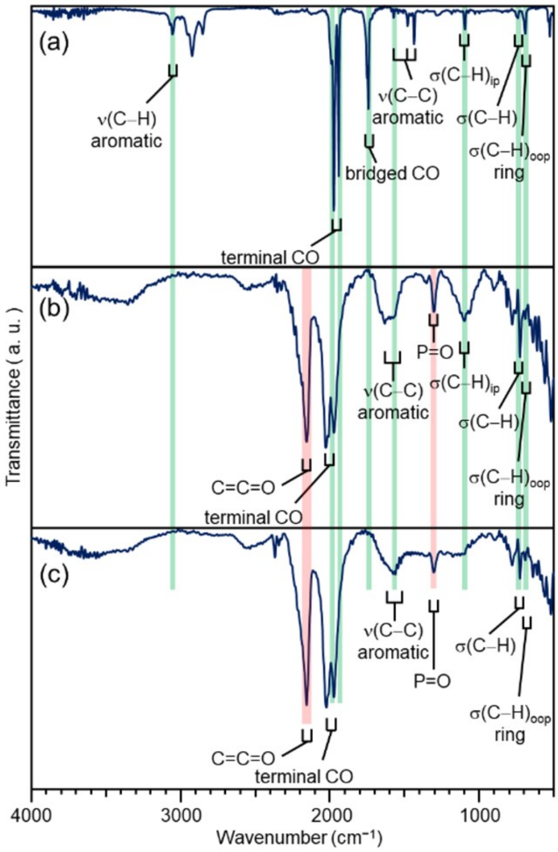

Fig. S10 Details of the assignments of FT-IR spectra. (a) $[Pt_{17}(CO)_{12}(PPh_3)_8]^z$. (b) $Pt_{17}(CO)_{12}(PPh_3)_8$/CB(1.0 wt% Pt). (c) Pt/CB(1.0 wt% Pt)

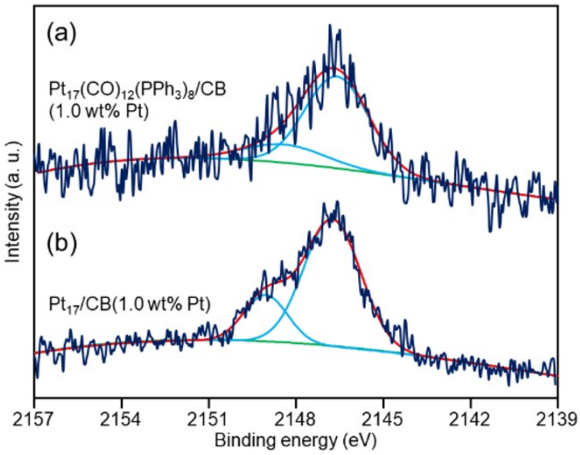

Fig. S11 Hard X-ray Photoelectron Spectroscopy (HAX-PES) spectra of P 1s. (a) $Pt_{17}(CO)_{12}(PPh_3)_8$/CB(1.0 wt% Pt). (b) Pt_{17}/CB(1.0 wt% Pt). The spectrum of $Pt_{17}(CO)_{12}(PPh_3)_8$/CB(1.0 wt% Pt) (a) indicate that a part of PPh_3 was oxidized when $Pt_{17}(CO)_{12}(PPh_3)_8$ was adsorbed onto CB. The oxidized product ($O{=}PPh_3$) is likely to move from the surface of Pt_{17} to that of CB. The spectrum of Pt_{17}/CB(1.0 wt% Pt) (b) demonstrates that 1) the oxidation of PPh_3 became more prominent after the calcination at 200 °C and 2) PPh_3 still exist in the catalysts even after the calcination at 200 °C although the amounts were not so large when considering the electron intensity. On the basis of the result of TGA (Fig. S18), the dissociation of P—C bond in PPh_3 seems to occur at the calcination of 200 °C. The resulting O=P is readily oxidized under the reduced pressure to produce P_4O_6 (boiling point = 173 ℃)[16], etc. and those phosphorus oxides seems to be vaporized at the 200 °C. This seems to be the reason why the electron intensity of P 1s spectrum of Pt_{17}/CB(1.0 wt% Pt) was weak.

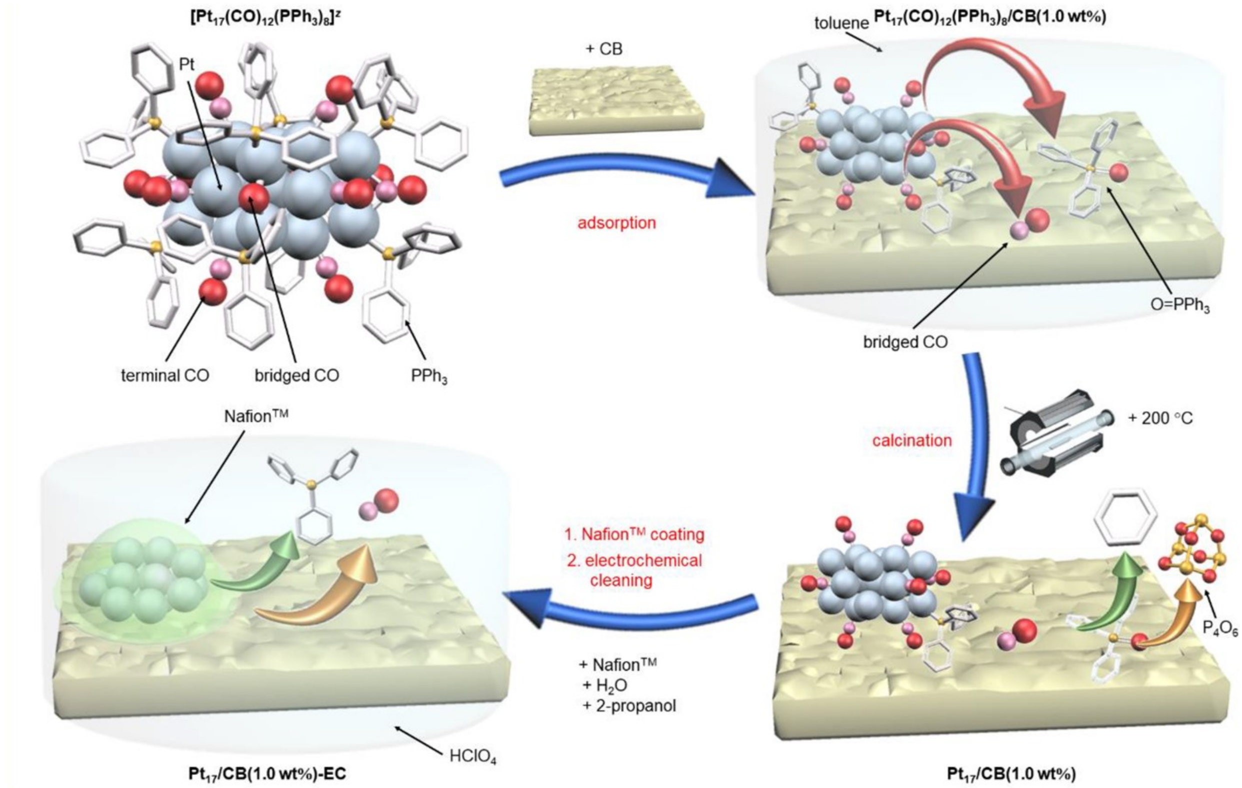

Fig. S12 Proposed ligand-elimination process. Regarding the adsorption process, FT-IR spectra (Fig. 3 and S10) indicate that: 1) bridged CO are desorbed from the surface of Pt_{17} (disappearance of the peak at 1742.4 cm^{-1}) and the detached CO forms the bond with the surface of CB (appearance of the peak at 2158.0 cm^{-1}); 2) part of PPh_3 are oxidized to O=PPh_3 (appearance of the peak at 1303.5 cm^{-1}), which remains in the catalysts. The oxidation of part of PPh_3 to O=PPh_3 is also supported by HA-XPS P 1s spectra (a peak at 2149 eV; Fig. S11). Pt L_3-edge FT-EXAFS spectrum indicates that the unoxidized PPh_3 is still attached on the surface of Pt_{17} (peak at ~2.25 Å; Fig. 4(a)). Since the peaks assigned to the ν(C—C) aromatic shifted in FT-IR spectrum of the sample after the adsorption (Fig. 3 and S10), it can be considered that the position of PPh_3 on Pt_{17} shifted from the original position in the precursor NCs to probably the periphery of Pt_{17}, where PPh_3 can interact with both Pt_{17} and CB and thereby PPh_3 can be more stabilized. Considering these facts, the upper left schematic is proposed as a model for the catalysts after adsorption. Regarding the calcination process, FT-IR spectra (Fig. 3 and S10) indicate that the total quantities of PPh_3 and O=PPh_3 in the catalysts decreased by the calcination. According to the thermogravimetric analysis (Fig. S18), P—C dissociation should occur by the calcination at 200 °C. The resulting O=P is readily oxidized under the reduced pressure to produce P_4O_6 (boiling point = 173 °C)[16], etc. and those phosphorus oxides seems to be vaporized at the 200 °C as described in the caption of Fig. S11. These chemical reactions are considered the reasons why the total quantities of PPh_3 and O=PPh_3 decreased by the calcination. Based on the Pt L_3-edge FT-EXAFS spectra (Fig. 4a), the calcination caused the formation of Pt—C bond (appearance of clear peak at ~1.7 Å) between Pt_{17} and CB, resulting in the immobilization of Pt_{17} on CB (appearance of clear peak at ~2.7 Å). On the other hand, FT-IR (Fig. 3 and S10) and HAX-PES P 1s spectra (Fig. S11) also imply that PPh_3 and O=PPh_3 could not be eliminated by the calcination at 200 °C. According to Pt L_3-edge FT-EXAFS spectrum (peak at ~2.25 Å; Fig. 4a), part of PPh_3 existed also on the surface of Pt_{17} after calcination (probably, part of PPh_3 is immobilized at the periphery of Pt_{17} by interacting with both Pt_{17} and CB; Fig. 3 and S10). Considering these facts, the lower left schematic is proposed as a model for the catalysts after calcination. However, the further experiments are needed to confirm the proposed ligand elimination process at molecular level[17], which exceeds the purpose of the present study.

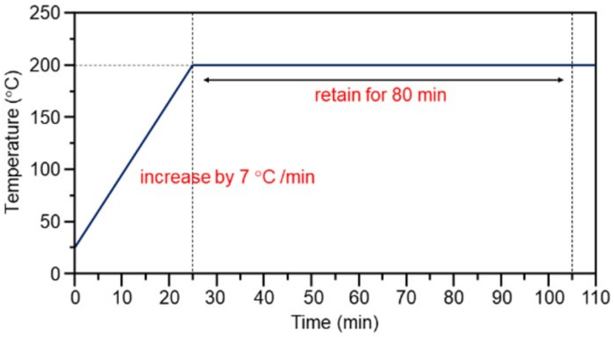

Fig. S13 Calcination program used in this work.

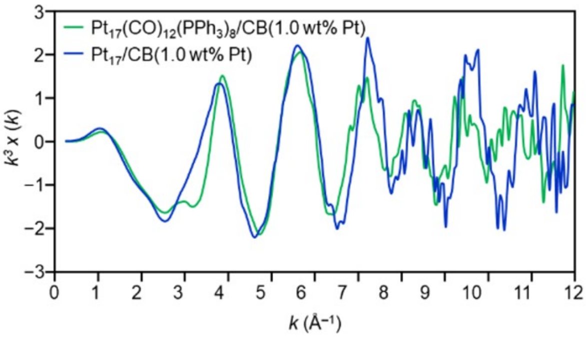

Fig. S14 Extended X-ray absorption fine structure (EXAFS) spectra of $Pt_{17}(CO)_{12}(PPh_3)_8$/CB(1.0 wt% Pt) and Pt_{17}/CB(1.0 wt% Pt). For Pt foil and PtO_2 powder, see Fig. S20.

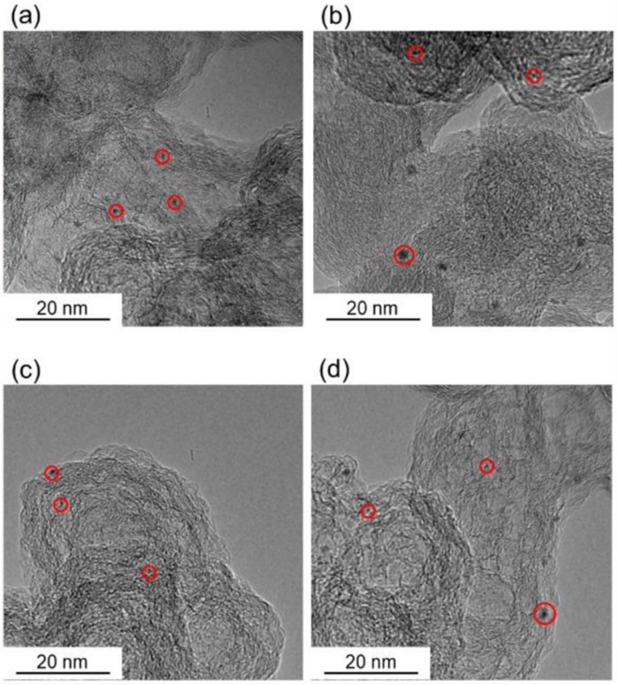

Fig. S15 TEM images of Pt_{17}/CB. (a–d) Different views from Fig. 2(c).

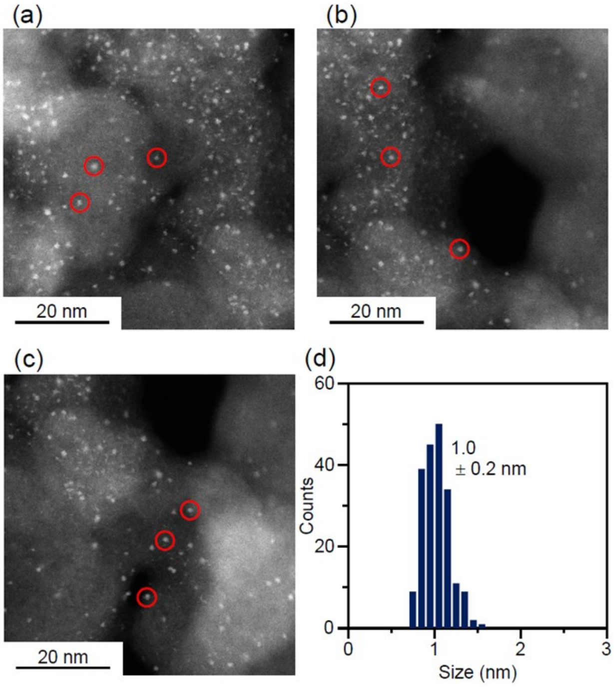

Fig. S16 HAADF-STEM images of Pt_{17}/CB and the histogram of Pt_{17}/CB. Overall, the particle sizes are similar to those in Figure S15.

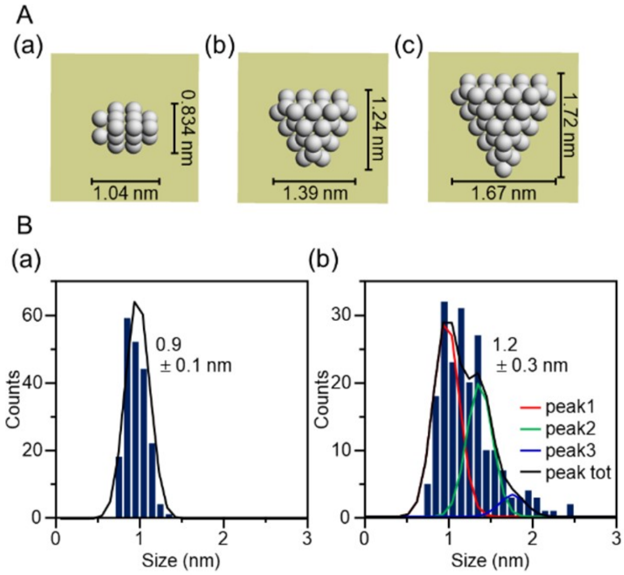

Fig. S17 Analysis of TEM images of Pt_{17}/CB. (A) Proposed geometrical structures and calculated diameters of the loaded metal clusters: (a) Pt_{17}, (b) Pt_{34} which could be produced by the fusion of two Pt_{17}, and (c) Pt_{51} which could be produced by the fusion of three Pt_{17}. (B) The results of curve fitting for the histograms (a) $Pt_{17}(CO)_{12}(PPh_3)_8$/CB (Fig. 2(b)) and (b) Pt_{17}/CB (Fig. 2(c)). In (b), the median value of peak 1, 2, and 3 correspond to the size of Pt_{17} (Fig. S17(a)), Pt_{34} (Fig. S17(b)), and Pt_{51} (Fig. S17(c)), respectively. These results imply that Pt_{17}, Pt_{34}, and Pt_{51} are included in Pt_{17}/CB at the ratio of 55.8, 37.9 and 6.3%, respectively, namely, the major NCs are Pt_{17}.

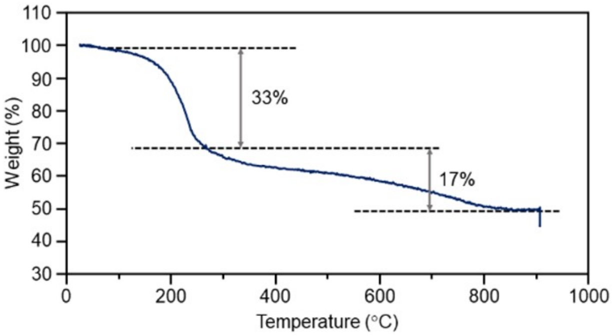

Fig. S18 Thermogravimetric analysis data for $[Pt_{17}(CO)_{12}(PPh_3)_8]Cl_n$ (n = 1 or 2). The weight of $[Pt_{17}(CO)_{12}(PPh_3)_8]Cl_n$ was decreased by two steps. The first decrease seems to be due to the vaporization of Cl and Ph_3 caused by the P—C dissociation (calculated weight loss is 33%), whereas the second decrease the vaporization of the remaining P and CO (calculated weight loss is 10%), although TG-MS is needed for the conformation of this assignments.

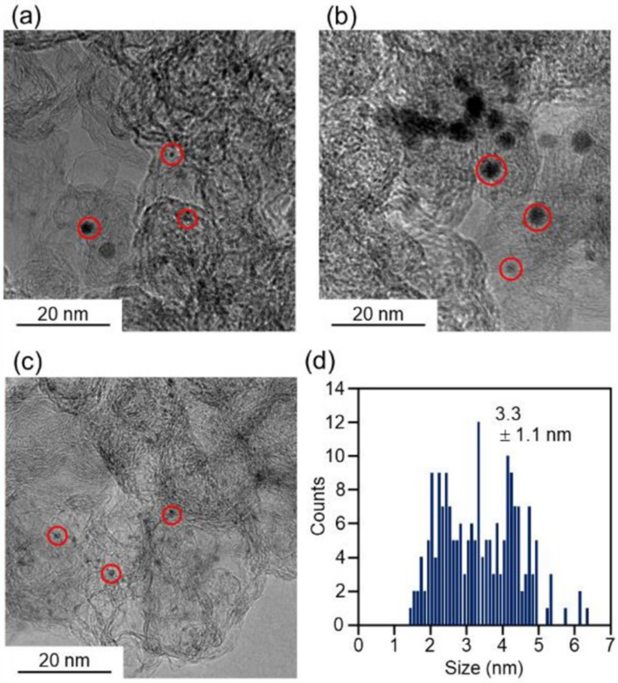

Fig. S19 TEM images and the histogram of Pt_{17}/CB(1.0 wt% Pt) prepared by the calcination at 400 ℃. (a–c) TEM images. (d) histogram. The remarkable aggregation of Pt_{17} NCs occurred by the calcination at 400 ℃.

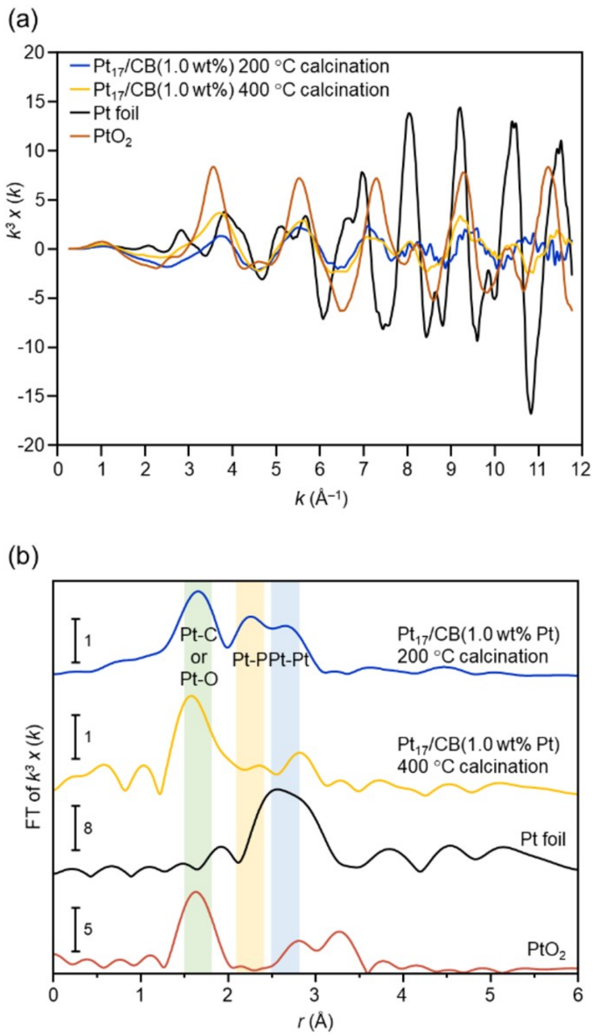

Fig. S20 EXAFS results for Pt_{17}/CB(1.0 wt% Pt) calcined at 400 °C. (a) EXAFS data. (b) FT-EXAFS spectra. In (a) and (b), the results obtained for Pt_{17}/CB(1.0 wt% Pt) calcined at 400 °C, Pt foil and PtO_2 are also shown for the comparison. In EXAFS spectra of Pt_{17}/CB(1.0 wt% Pt) calcined at 400 °C, the peak attributed to Pt—P was almost nonexistent, indicating that P was perfectly removed from the surface of Pt NCs, different from the case of the calcination at 400 °C. However, as shown in Fig. S19, the remarkable aggregation of Pt_{17} NCs occurred by the calcination at 400 °C, which is consistent with the result on the FT-EXAFS that the peaks attributed to Pt—Pt appeared in the FT-EXAFS spectrum of Pt_{17}/CB(1.0 wt% Pt) calcined at 400 °C clearly than in that of Pt_{17}/CB(1.0 wt% Pt) calcined at 200 °C. Therefore, it can be judged that the calcination temperature suitable for the loading of Pt_{17} while keeping their particle size is 200 °C.

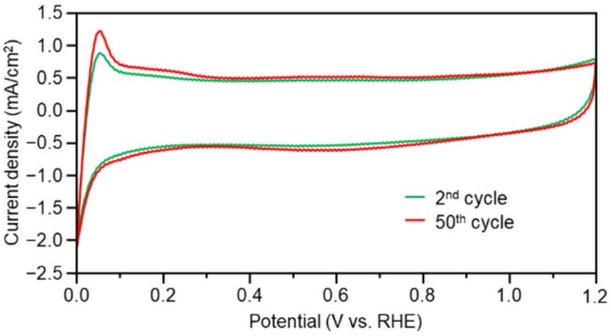

Fig. S21 Cyclic voltammetry (CV) curves of Pt_{17}/CB(1.0 wt% Pt) after 2 or 50-time cycling. CV curve changes slightly after 2 or 50-time cycling, implying that the residual organic molecules were removed from the surface of Pt_{17} NCs by the electrochemical cleaning. In these curves, the intensities of peaks attributed to the electrochemically active surface area (ECSA; 0.1–0.4 V; Fig. S24(b)) were quite weak since the loading amounts of Pt was quite low (1.0 wt% Pt). Accordingly, the ECSA could not be estimated for Pt_{17}/CB(1.0 wt% Pt).

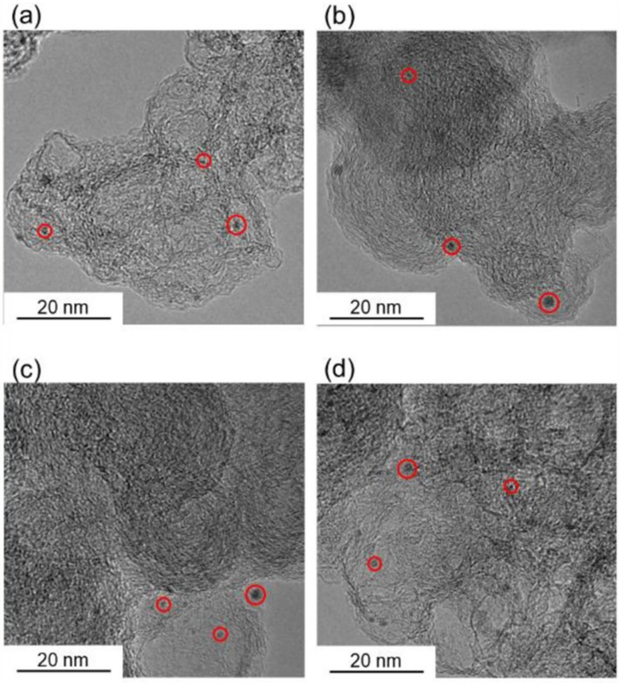

Fig. S22 TEM images of Pt_{17}/CB(1.0 wt% Pt)-EC. (a–d) Different views. Only negligible agglomeration occurred by the electrochemical cleaning.

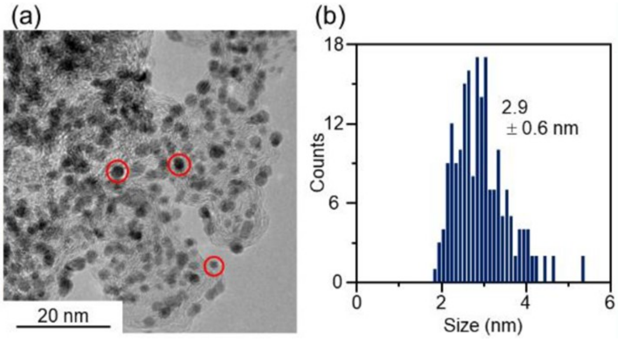

Fig. S23 TEM images and the histogram of commercial Pt NPs/CB(46.9 wt% Pt). (a) TEM images. (b) histogram. The observed particle sizes are well consistent with the reported ones[18].

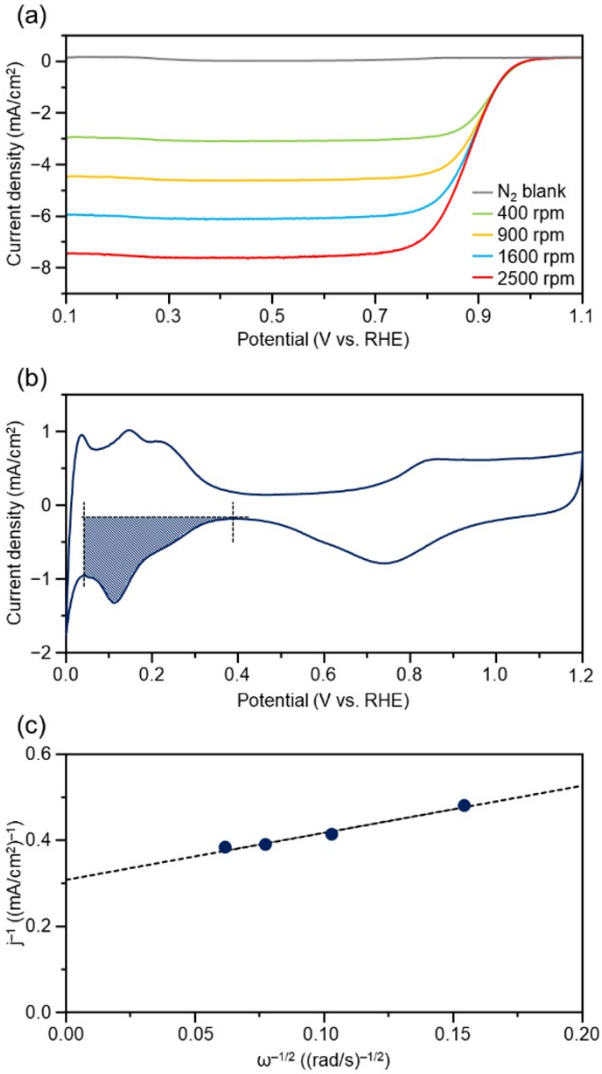

Fig. S24 Electrochemical results for Pt NPs/CB(46.9 wt% Pt)-EC. In these measurements, Pt loading was set to 17.8 μg/cm^2. (a) LSV curves obtained for electrode rotation speeds of 400−2500 rpm under O_2 gas. The measurements under N_2 gas were conducted for baseline comparison. (b) CV curve. The shadow area originates from the hydrogen adsorption[19]. Electrochemically active surface area (ECSA) of catalyst was estimated based on this area. (c) Koutecky-Levich plots[20]. The number of the transferred electrons and the mass activity (~182 A/g for 0.9 V) were calculated on the basis of these results.

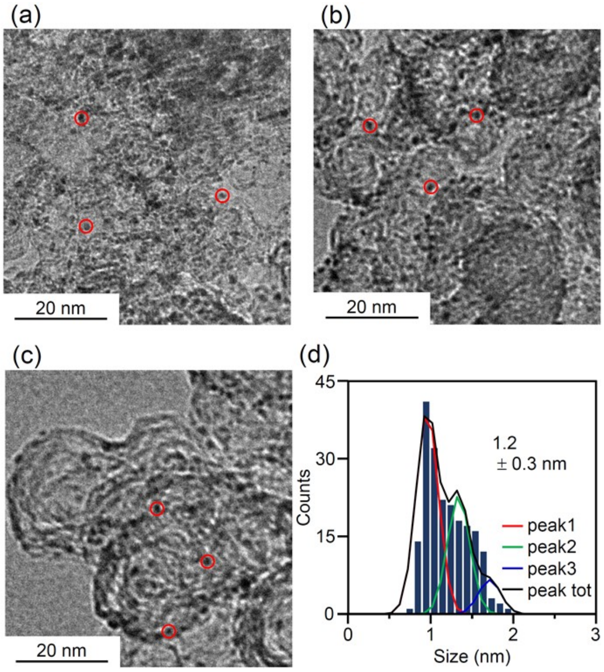

Fig. S25 TEM images of Pt_{17}/CB(20.0 wt% Pt). (a−c) TEM images. (d) histogram. In (d), the results of curve fitting for the histograms is also shown. In (d), the median value of peak 1, 2, and 3 correspond to the size of Pt_{17} (Fig. S17(a)), Pt_{34} (Fig. S17(b)), and Pt_{51} (Fig. S17(c)), respectively. These results imply that Pt_{17}, Pt_{34}, and Pt_{51} are included in Pt_{17}/CB at the ratio of 57.2, 33.2 and 9.59%, respectively, namely, the major NCs are Pt_{17}.

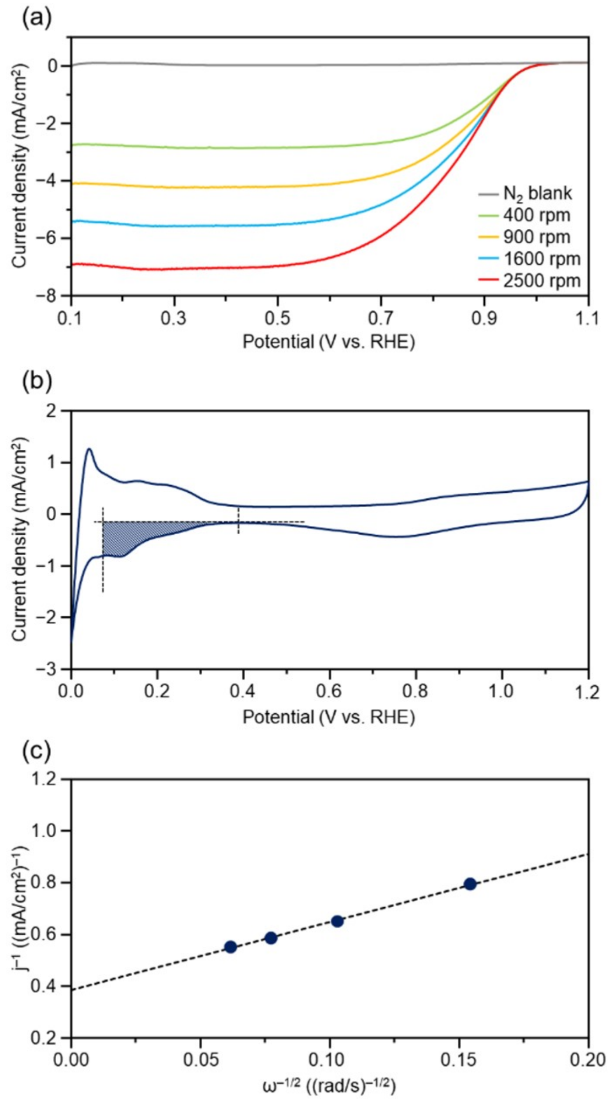

Fig. S26 Electrochemical results for Pt_{17}/CB(20.0 wt% Pt)-EC. In these measurements, Pt loading was set to 5.05 μg/cm^2. (a) LSV curves obtained for electrode rotation speeds of 400−2500 rpm under O_2 gas. The measurements under N_2 gas were conducted for baseline comparison. (b) CV curve. The shadow area originates from the hydrogen adsorption[19]. Electrochemically active surface area (ECSA) of catalyst was estimated based on this area. (c) Koutecky-Levich plots[20]. The number of the transferred electrons (~4e) and the mass activity (518 A/g for 0.9 V) were calculated on the basis of these results.

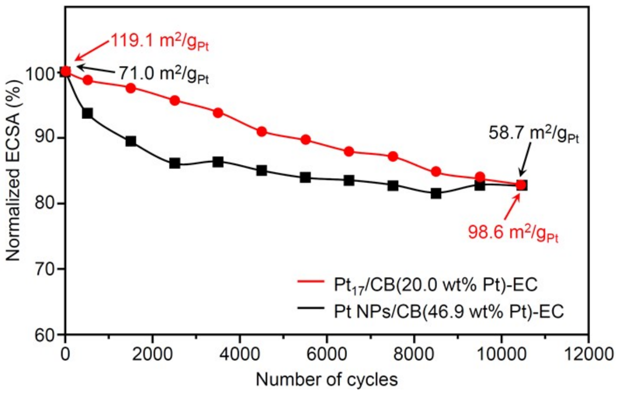

Fig. S27 Normalized ECSA of Pt_{17}/CB(20.0 wt% Pt)-EC and commercial Pt NPs/CB (46.9 wt% Pt) during accelerated durability test. This result demonstrates that Pt_{17}/CB(20.0 wt% Pt)-EC exhibits higher durability than commercial Pt NPs/CB (46.9 wt% Pt).

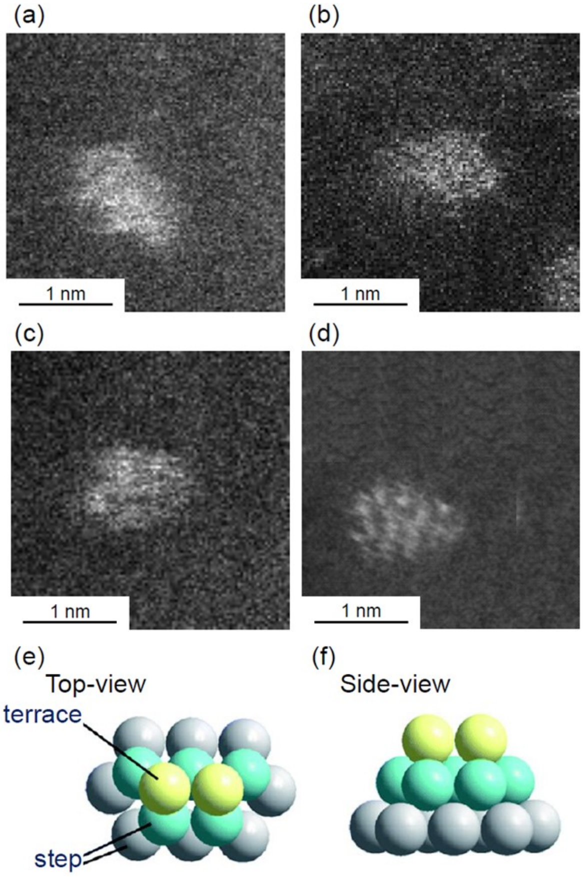

Fig. S28 HAADF-STEM images and model structure of Pt_{17} on the substrate. HAADF-STEM images of (a-c) Pt_{17}/CB(1.0 wt% Pt) and (d) Pt_{17}/γ-alumina (0.15 wt% Pt)[21]. (e,f) Model structure predicted from the HAADF-STEM image of Pt_{17}/γ-alumina (0.15 wt% Pt)[21]. Unfortunately, each Pt atom could not be observed even in the enlarged views for Pt_{17}/CB(1.0 wt% Pt) . However, the overall morphology of Pt_{17} in Pt_{17}/CB(1.0 wt% Pt) was similar to that in Pt_{17}/γ-alumina (0.15 wt% Pt). In addition, the geometry of Pt_{17}/graphite was optimized in this study. Accordingly, it can be considered that the theoretical cluster model is reasonable.

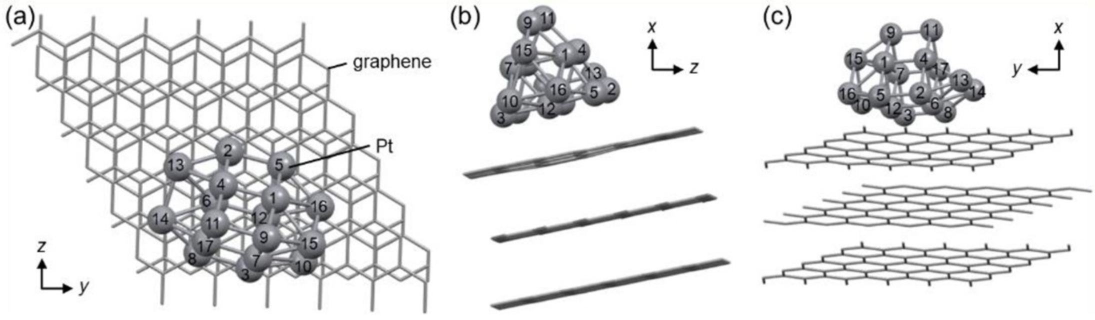

Fig. S29 Optimized structure for Pt_{17}/graphite. (a–c) Different views from Fig. 6(a).

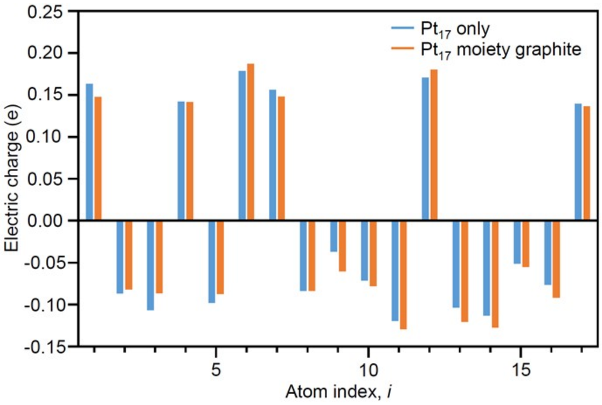

Fig. S30 Electric charge of each Pt atom in isolated Pt$_{17}$ and Pt$_{17}$/graphite. (blue) isolated Pt17 and (red) Pt$_{17}$ moiety on graphite. The atom index (*i*) of each Pt atom is described in Fig. 6(a). This comparison indicates that the graphene plays a minor role in the present ORR due to the weak chemical bonds between graphite and Pt cluster.

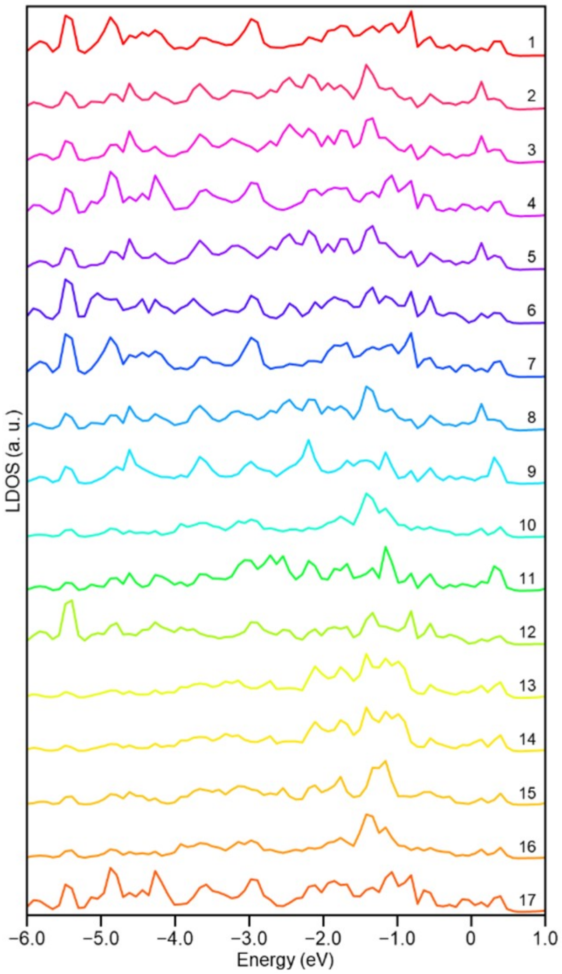

Fig. S31 Local density of states (LDOS) of each Pt atom for Pt$_{17}$/graphite. The atom index (*i*) of each Pt atom is shown in Fig. 6(a) and S29.

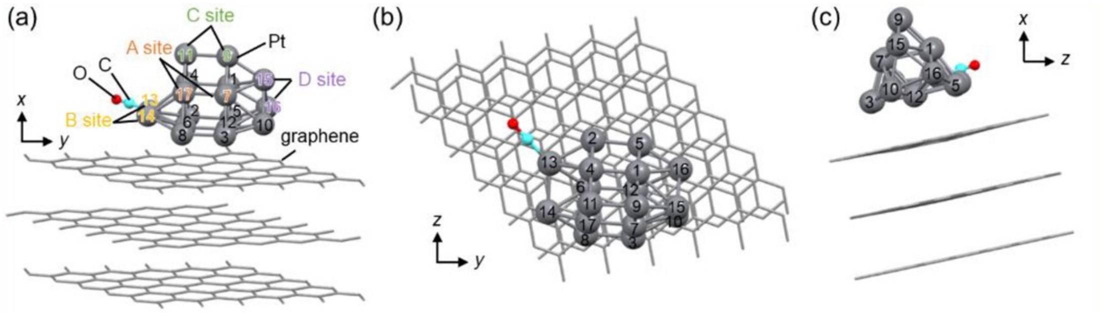

Fig. S32 Optimized structure for CO/Pt$_{17}$/graphite. (a–c) Different views, respectively.

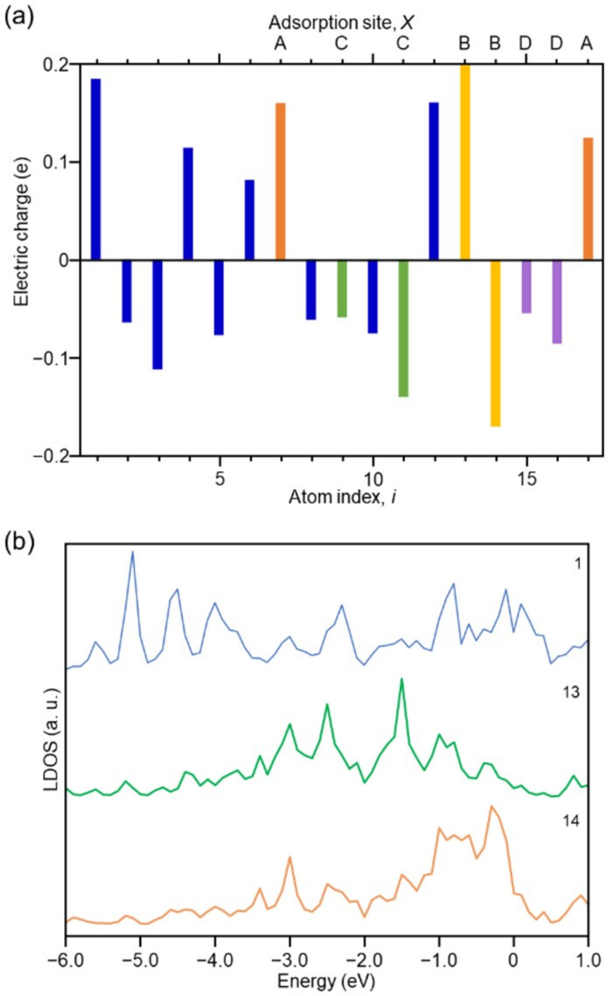

Fig. S33 Electronic structure of each Pt atom for CO/Pt$_{17}$/graphite. (a) Electric charge of each Pt atom. (b) LDOS for the several Pt atoms. The atom index (i) of each Pt atom is shown in Fig. S32.

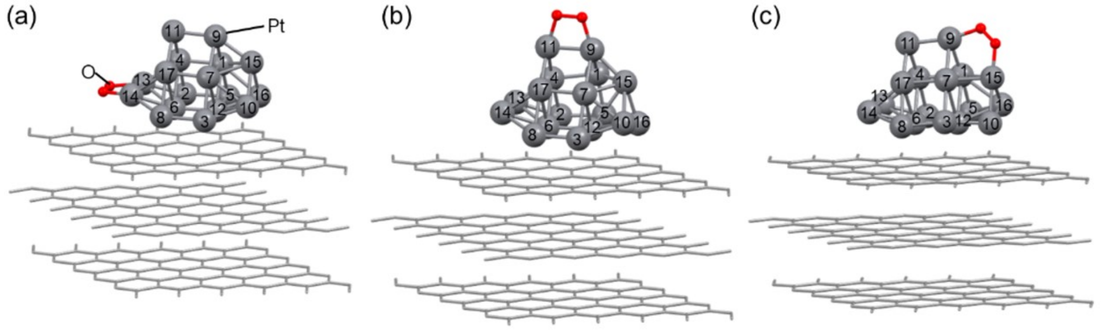

Fig. S34 Optimized structure for O$_2$/Pt$_{17}$/graphite. (a–c) Different views from Fig. 6(c).

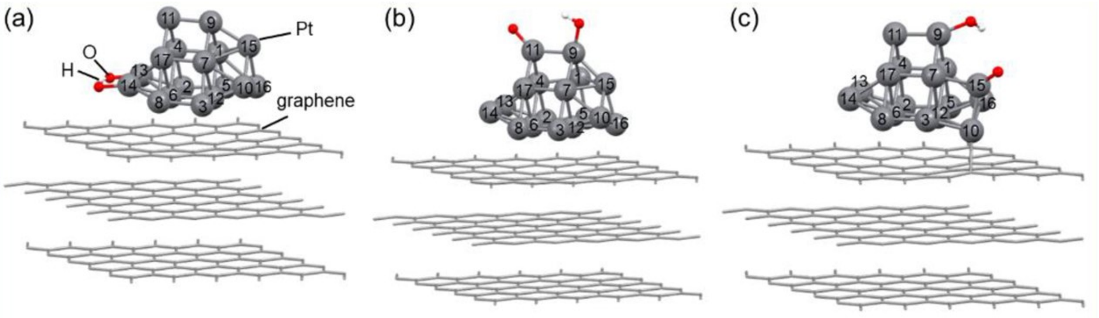

Fig. S35 Optimized structure for (O + OH)Pt_{17}/graphite. (a–c) Different views from Fig. 6(d).

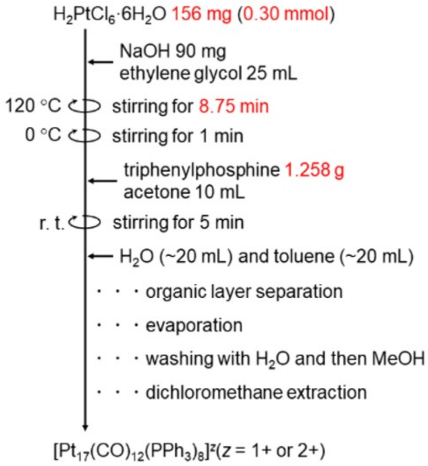

Fig. S36 Synthesis protocol of $[Pt_{17}(CO)_{12}(PPh_3)_8]^z$ (z = 1+ or 2+). The amounts of the reagents modified from our previous study are highlighted in red color.

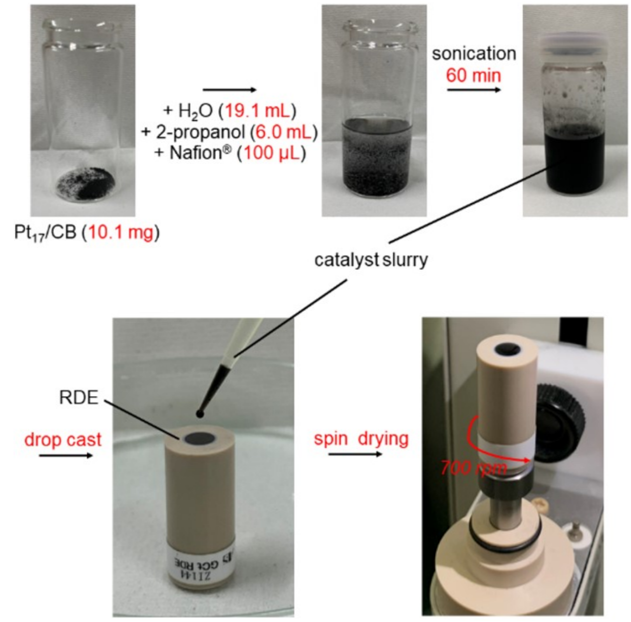

Fig. S37 Schematic of preparation of Pt_n/CB catalyst slurry and their loading on RDE. The experimental conditions modified from our previous study are highlighted in red color.

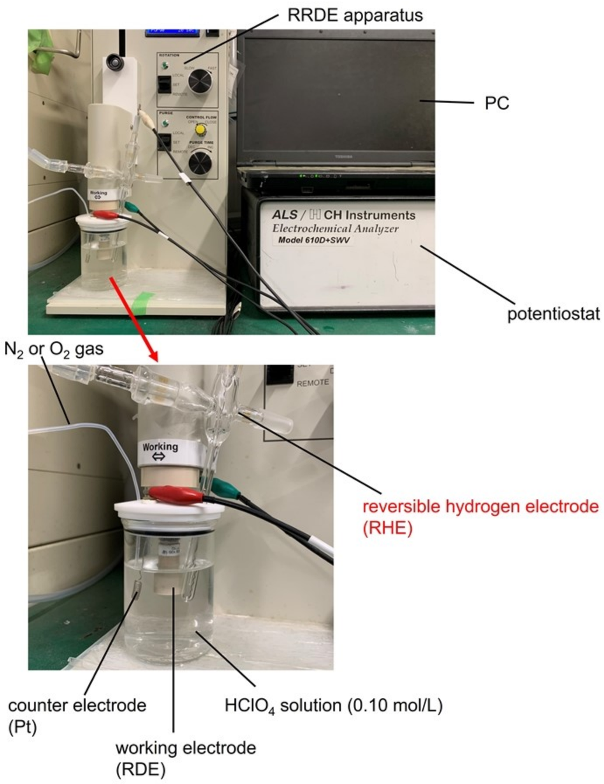

Fig. S38 Photographs of the apparatus used in this work for electrochemical experiments. The setup modified from our previous study (reference electrode) is highlighted in red color.

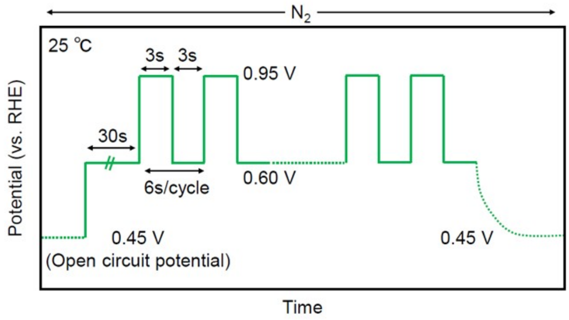

Fig. S39 Flow of the durability test used in this work.[22]

S5. References

1. L. V. Nair, S. Hossain, S. Wakayama, S. Takagi, M. Yoshioka, J. Maekawa, A. Harasawa, B. Kumar, Y. Niihori, W. Kurashige and Y. Negishi, *J. Phys. Chem. C,* **2017**, *121*, 11002−11009.
2. T. Kawawaki, N. Shimizu, K. Funai, Y. Mitomi, S. Hossain, S. Kikkawa, D. J. Osborn, S. Yamazoe, G. F. Metha and Y. Negishi, *Nanoscale,* **2021**, *13*, 14679−14687.
3. Y. Takagi, T. Uruga, M. Tada, Y. Iwasawa and T. Yokoyama, *Acc. Chem. Res.,* **2018**, *51*, 719−727.
4. T. Uruga, M. Tada, O. Sekizawa, Y. Takagi, T. Yokoyama and Y. Iwasawa, *Chem. Rec.,* **2019**, *19*, 1444−1456.
5. S. K. Eriksson, M. Hahlin, J. M. Kahk, I. J. Villar-Garcia, M. J. Webb, H. Grennberg, R. Yakimova, H. Rensmo, K. Edström, A. Hagfeldt, H. Siegbahn, M. O. M. Edwards, P. G. Karisson, K. Backlund, J. Åhlund and D. J. Payne, *Rev. Sci. Instrum.,* **2014**, *85*, 075119.
6. J. P. Perdew, K. Burke and M. Ernzerhof, *Phys. Rev. Lett.,* **1996**, *77*, 3865.
7. J. P. Perdew, K. Burke and M. Ernzerhof, *Phys. Rev. Lett.,* **1997**, *78*, 1396.
8. P. Giannozzi, S. Baroni, N. Bonini, M. Calandra, R. Car, C. Cavazzoni, D. Ceresoli, G. L. Chiarotti, M. Cococcioni, I. Dabo, A. D. Corso, S. de Gironcoli, S. Fabris, G. Fratesi, R. Gebauer, U. Gerstmann, C. Gougoussis, A. Kokalj, M. Lazzeri, L. Martin-Samos, N. Marzari, F. Mauri, R. Mazzarello, S. Paolini, A. Pasquarello, L. Paulatto, C. Sbraccia, S. Scandolo, G. Sclauzero, A. P. Seitsonen, A. Smogunov, P. Umari and R. M. Wentzcovitch *J. Phys.: Condens. Matter,* **2009**, *21*, 395502.
9. S. Grimme, J. Antony, S. Ehrlich and H. Krieg, *J. Chem. Phys.,* **2010**, *132*, 154104.
10. J. K. Nørskov, J. Rossmeisl, A. Logadottir, L. Lindqvist, J. R. Kitchin, T. Bligaard and H. Jónsson, *J. Phys. Chem. B,* **2004**, *108*, 17886−17892.
11. J. Rossmeisl, A. Logadottir and J. K. Nørskov, *Chem. Phys.,* **2005**, *319*, 178−184.
12. D.-H. Lim and J. Wilcox, *J. Phys. Chem. C,* **2012**, *116*, 3653−3660.
13. H. G. M. Edwards, A. F. Johnson and I. R. Lewis, *Spectrochim. Acta, Part A,* **1993**, *49A*, 707−714.
14. T. Kawawaki, Y. Kataoka, S. Ozaki, M. Kawachi, M. Hirata and Y. Negishi, *Chem. Commun.,* **2021**, *57*, 417−440.
15. S. S. Kurasov, N. K. Eremenko, Y. L. Slovokhotov and Y. T. Struchkov, *J. Organomet. Chem.,* **1989**, *361*, 405−408.
16. https://www.lookchem.com/CASDataBase_12440-00-5.htm **2008**.
17. T. Kawawaki, Y. Kataoka, M. Hirata, Y. Akinaga, R. Takahata, K. Wakamatsu, Y. Fujiki, M. Kataoka, S. Kikkawa, A. S. Alotabi, S. Hossain, D. J. Osborn, T. Teranishi, G. G. Andersson, G. F. Metha, S. Yamazoe and Y. Negishi, *Angew. Chem., Int. Ed.,* **2021**, *60*, 21340−21350.
18. J. Bucher, J. Quinson, A. M. Mingers, D. Zhang and M. Arenz, *Anal. Chim. Acta,* **2020**, *1101*, 41−49.
19. K. J. J. Mayrhofer, D. Strmcnik, B. B. Blizanac, V. Stamenkovic, M. Arenz and N. M. Markovic, *Electrochim. Acta,* **2008**, *53*, 3181−3188.
20. M. Li, Z. Zhao, T. Cheng, A. Fortunelli, C.-Y. Chen, R. Yu, Q. Zhang, L. Gu, B. V. Merinov, Z. Lin, E. Zhu, T. Yu, Q. Jia, J. Guo, L. Zhang, W. A. Goddard, Y. Huang and X. Duan, *Science,* **2016**, *354*, 1414−1419.
21. Y. Negishi, N. Shimizu, K. Funai, R. Kaneko, K. Wakamatsu, A. Harasawa, S. Hossain, M. E. Schuster, D. Ozkaya, W. Kurashige, T. Kawawaki, S. Yamazoe and S. Nagaoka, *Nanoscale Adv.*, **2020**, *2*, 669−678.
22. M. Mench, E. C. Kumbur and T. N. Veziroglu, Polymer electrolyte fuel cell degradation; *Academic Press*, Cambridge, **2011**.